(This is a sample cover image for this issue. The actual cover is not yet available at this time.)

Biochimica et Biophysica Acta 1818 (2012) 877–888

Contents lists available at SciVerse ScienceDirect

Biochimica et Biophysica Acta

journal homepage: www.elsevier.com/locate/bbamem

S4(13)-PV cell-penetrating peptide induces physical and morphological changes in membrane-mimetic lipid systems and cell membranes: Implications for cell internalization

Ana M.S. Cardoso [a], Sara Trabulo [a], Ana L. Cardoso [a], Annely Lorents [b], Catarina M. Morais [a], Paula Gomes [c], Cláudia Nunes [d], Marlene Lúcio [d], Salette Reis [d], Kärt Padari [b], Margus Pooga [b], Maria C. Pedroso de Lima [a,e], Amália S. Jurado [a,e,*]

[a] CNC - Centre for Neuroscience and Cell Biology, University of Coimbra, Portugal
[b] Institute of Molecular and Cell Biology, University of Tartu, Tartu, Estonia
[c] Centre for Chemistry Investigation, Department of Chemistry, Faculty of Sciences, University of Porto, Portugal
[d] REQUIMTE, Departamento de Química, Faculdade de Farmácia, Universidade do Porto, Portugal
[e] Department of Life Sciences, University of Coimbra, Portugal

ARTICLE INFO

Article history:
Received 22 September 2011
Received in revised form 5 December 2011
Accepted 21 December 2011
Available online 31 December 2011

Keywords:
Cell-penetrating peptide
Membrane model
DSC
Fluorescence polarization
WAXS/SAXS
Electron microscopy

ABSTRACT

The present work aims to gain insights into the role of peptide–lipid interactions in the mechanisms of cellular internalization and endosomal escape of the S4(13)-PV cell-penetrating peptide, which has been successfully used in our laboratory as a nucleic acid delivery system. A S4(13)-PV analogue, S4(13)-PVscr, displaying a scrambled amino acid sequence, deficient cell internalization and drug delivery inability, was used in this study for comparative purposes. Differential scanning calorimetry, fluorescence polarization and X-ray diffraction at small and wide angles techniques showed that both peptides interacted with anionic membranes composed of phosphatidylglycerol or a mixture of this lipid with phosphatidylethanolamine, increasing the lipid order, shifting the phase transition to higher temperatures and raising the correlation length between the bilayers. However, S4(13)-PVscr, in contrast to the wild-type peptide, did not promote lipid domain segregation and induced the formation of an inverted hexagonal lipid phase instead of a cubic phase in the lipid systems assayed. Electron microscopy showed that, as opposed to S4(13)-PVscr, the wild-type peptide induced the formation of a non-lamellar organization in membranes of HeLa cells. We concluded that lateral phase separation and destabilization of membrane lamellar structure without compromising membrane integrity are on the basis of the lipid-driven and receptor-independent mechanism of cell entry of S4(13)-PV peptide. Overall, our results can contribute to a better understanding of the role of peptide–lipid interactions in the mechanisms of cell-penetrating peptide membrane translocation, helping in the future design of more efficient cell-penetrating peptide-based drug delivery systems.

1. Introduction

Cell-penetrating peptides (CPPs) constitute an expanding peptide family whose members share the ability to cross biological membranes and gain access into living cells [1,2]. Although biomembranes are generally impermeable to large or highly charged molecules, accumulating evidences have demonstrated the capacity of CPPs to mediate intracellular delivery of a wide variety of exogenous charged molecules, especially peptides and proteins [1,3] and nucleic acids, such as splice correcting oligonucleotides [4], siRNA [1,5] and plasmid DNA [6]. Thus, CPPs opened new possibilities in biomedical research and therapy, offering new tools for intracellular delivery of drugs or genetic cargo as an alternative to the conventional pharmaceutical approaches involving viral vectors [7], lipid-based carriers [8] and physical methods to enhance internalization of therapeutic molecules into cells [9].

Although CPPs have been widely used to deliver cargo molecules into cells, the mechanisms underlying CPP cellular uptake are far from being fully understood. Several endocytotic and non-endocytotic pathways for CPP internalization have been proposed depending on CPP own features, the carried cargo, the cell type and the membrane lipid composition [1,2]. In this context, the interactions between CPPs and

Abbreviations: CPP, cell-penetrating peptide; DOPE, 1,2-dioleoyl-sn-glycero-3-phosphoethanolamine; DOPG, 1,2-dioleoyl-sn-glycero-3-phospho-(1′-rac-glycerol); DPH-PA, 3-(p-(6-phenyl)-1,3,5-hexatrienyl)phenylpropionic acid; DPPC, 1,2-dipalmitoyl-sn-glycero-3-phosphocholine; DPPE, 1,2-dipalmitoyl-sn-glycero-3-phosphoethanolamine; DPPG, 1,2-dipalmitoyl-sn-glycero-3-phospho-(1′-rac-glycerol); DSC, differential scanning calorimetry; LUV, large unilamellar vesicles; MLV, multilamellar vesicles; POPG, 1-palmitoyl-2-oleoyl-sn-glycero-3-phospho-(1′-rac-glycerol); SAXS, small angle X-ray scattering; WAXS, wide angle X-ray scattering; 2-AS, 2-(9-anthroyloxy) stearic acid; 6-AS, 6-(9-anthroyloxy) stearic acid; 12-AS, 12-(9-anthroyloxy) stearic acid and 16-AP, 16-(9-anthroyloxy) palmitic acid

* Corresponding author at: Centre for Neuroscience and Cell Biology, University of Coimbra, Largo Marquês de Pombal, 3004-517 Coimbra, Portugal. Tel.: +351 239 853600; fax: +351 239 853607.
E-mail address: asjurado@bioq.uc.pt (A.S. Jurado).

0005-2736/$ – see front matter © 2011 Elsevier B.V. All rights reserved.
doi:10.1016/j.bbamem.2011.12.022

membrane lipids have been suggested to play a major role in CPP membrane translocation [1]. With respect to the membrane, the transverse as well as the lateral structure of the membrane lipid bilayer assume high relevance. Membrane outer regions, with a high density of negative charges mainly conferred by membrane-associated glycosaminoglycan (GAG)-linked proteins (proteoglycans) or neuraminic acid-containing oligosaccharides attached to membrane embedded glycoproteins and gangliosides, may establish electrostatic interactions with the positively charged regions of CPPs resulting from the high density of basic amino acid residues (e.g. Arg and Lys) [1]. On the other hand, the hydrophilic–hydrophobic interface of the lipid bilayer interacts with the amphiphilic portions of the peptides, modulating their folding/unfolding and hence their membrane penetration. The heterogeneous lateral structure of the lipid bilayer and the lipid-microdomain organization are not less important in terms of membrane transposition by CPP molecules, since domain boundaries enhance bilayer permeability and may favor the insertion of those foreign molecules [10].

In order to study the role of CPP–lipid interactions in translocation of CPP-conjugated drug delivery systems through the cell membrane, different biophysical approaches have been adopted, most of them using membrane models [11–14]. These simple experimental systems have allowed addressing the influence of structural and physical features of CPPs and their conjugates in the efficiency of the delivery process. In this regard, the amino acid composition and sequence, as well as the peptide conformation, have been shown to be important features of CPPs towards the success of cargo delivery [2]. Moreover, the size, the interfacial properties of CPP-based drug delivery systems and other physical characteristics, such as hydrophobicity/hydrophilicity and surface charge of the vectors or their components, can significantly influence their interactions with membrane lipids, and hence the efficiency of vector internalization [1,15,16]. On the other hand, studies of CPP–lipid interactions in membrane models manipulated to mimic biomembranes have shown the importance of the degree of lipid saturation, the cholesterol content and the membrane local charge on the ability of the peptide to interact, disturb and penetrate model membranes [17–19].

The peptide S4(13)-PV, a chimeric CPP containing a cell-penetrating sequence of 13 amino acids derived from Dermaseptin S4 peptide and the nuclear localization signal of the simian virus 40 (SV40) large T antigen [2], has shown to be efficiently taken up by cells through an apparently receptor- and energy-independent process and, less efficiently, through clathrin-mediated endocytosis [16,20]. The high translocation ability of S4(13)-PV peptide across cell membranes is reflected in its competence to generate nucleic acid carrier systems with great potential to deliver plasmid DNA [6], splice switching oligonucleotides [4] and siRNA (unpublished data). However, these features are not fully shared by its analogue [S4(13)-PV_{scr}], which displays a scrambled sequence and was herein used for comparison, hence reflecting the relevance of the cell penetrating amino acid sequence and resulting α-helical conformation upon membrane interaction for translocation and biological activity [16].

In the present study, biophysical and ultrastructural studies were performed to characterize membrane interactions of the wild type S4(13)-PV peptide [S4(13)-PV_{wt}] and its scrambled analogue in order to uncover the mechanisms underlying their membrane translocation and ability for nucleic acid delivery, hence, contributing to the advance in the application of this CPP for therapeutic purposes.

2. Materials and methods

2.1. Chemicals

The lipids 1,2-dioleoyl-sn-glycero-3-phosphoethanolamine (DOPE), 1,2-dioleoyl-sn-glycero-3-phospho-(1′-rac-glycerol) (DOPG), 1,2-dipalmitoyl-sn-glycero-3-phosphoethanolamine (DPPE), 1,2-dipalmitoyl-sn-glycero-3-phosphocholine (DPPC), 1,2-dipalmitoyl-sn-glycero-3-phospho-(1′-rac-glycerol) (DPPG) and 1-palmitoyl-2-oleoyl-sn-glycero-3-phospho-(1′-rac-glycerol) (POPG) were purchased from Avanti Polar Lipids, Alabaster, AL. The fluorescent probes 3-(p-(6-phenyl)-1,3,5-hexatrienyl)phenylpropionic acid (DPH-PA), 2-(9-anthroyloxy) stearic acid (2-AS), 6-(9-anthroyloxy) stearic acid (6-AS), 12-(9-anthroyloxy) stearic acid (12-AS) and 16-(9-anthroyloxy) palmitic acid (16-AP) were obtained from Molecular Probes Inc. (Eugene, OR).

2.2. Peptides

Peptide S4(13)-PV [S4(13)-PV_{wt}, Table 1] was prepared as a C-terminal amide by solid-phase methodologies based on classical Fmoc (1-(9H-fluoren-9-yl)-methoxycarbonyl)/tert-Butyl chemistry [21], as previously described [6]. The scrambled peptide [S4(13)-PV_{scr}, Table 1] was generated on the basis of S4(13)-PV peptide sequence, so that the resulting peptide had the same amino acid composition and overall charge, but a distinct primary sequence. Both peptides were acetylated at their N-terminus and isolated in high purity level (>95%). Freeze-dried peptides were reconstituted in ultra-pure water. Concentration of S4(13)-PV peptides was determined by amino acid analysis and light absorption at 280 nm. Amino acid analysis was performed in a Beckman 6300 automatic analyzer, (CA, USA), following acid hydrolysis of the peptide.

2.3. Lipid preparations

Liposomes were prepared by hydration of lipid films as previously described [22]. Briefly, lipid films, resulting from the evaporation to dryness of aliquots of lipid solutions in chloroform (DPPC, DMPG, DPPG or a mixture of POPG/DPPE at 3/7 molar ratio) were hydrated with an appropriate volume of 50 mM KCl, 10 mM Tris–maleate buffer (pH 7.4) and liposome dispersions were obtained by handshaking in a water bath set 7–10 °C above the transition temperature of the phospholipids. Then, the suspensions of multilamellar vesicles were vortexed for 1 min to disperse aggregates. For DSC experiments, liposomal samples (75 mM in phospholipid) were used immediately after preparation. However, for spectrofluorimetric techniques, liposomes (200 μM in phospholipid) were subsequently sonicated in a low energy water sonifier for a few seconds to decrease the light scattered by the multilamellar vesicle (MLV) suspensions. For fluorescence polarization measurements, the probes (DPH-PA, 2-AS, 6-AS, 12-AS or 16-AP) were then incorporated in liposomes, by injecting a few microliters of the concentrated probe solution in dimethylformamide into liposome suspensions to obtain a lipid/probe molar ratio of 200/1. Thereafter, the liposome suspensions were incubated for 30 min in a water bath set 7–10 °C above the transition temperature of the phospholipids and let to stabilize overnight at room temperature, in the dark. Blank samples were prepared with equivalent volumes of the probe solvent.

For SAXS and WAXS measurements, lipid films obtained as described above were dried under a stream of N_2 and left overnight under reduced pressure to remove all traces of the organic solvents. The lipid films were hydrated with 50 mM KCl, 10 mM Tris–maleate buffer (pH 7.4) or buffered solutions of S4(13)-PV peptides (wt and scr) added to obtain lipid/peptide molar ratios from 50/1 to 100/1. Lipid suspensions were then heated above the lipid phase transition temperature in a water bath, mixed by vortexing for about 5 min and centrifuged for 30 s at 2000 *g*.

Table 1
Amino acid sequences of the $S4_{13}$-PV_{wt} and a scrambled analogue ($S4_{13}$-PV_{scr}) used in the present study.

$S4_{13}$-PV_{wt}	ALWKTLLKKVLKAPKKKRKVC-NH_2
$S4_{13}$-PV_{scr}	KTCKVAKWLKKAKPLRKLVKC-NH_2

This procedure was repeated three times. Finally, the samples were aged overnight at 4 °C and shaken under vortex at room temperature for 5 min. The dispersions were transferred into glass capillaries, transparent to X-rays, of 1.5 mm diameter (Hilgenberg, Malsfeld, Germany). The flame-sealed capillaries were stored at 4 °C until the time of the measurements.

2.4. DSC scans

The MLV suspensions incubated with peptide (peptide/lipid molar ratios in the range of 20/1 to 80/1) were sealed into aluminum pans. Heating scans were performed over an appropriate temperature range in a Perkin Elmer Pyris 1 differential scanning calorimeter, at a scan rate of 5 °C min^{-1}. To check the reproducibility of data, three heating scans were recorded for each sample. Data acquisition and analysis were performed using the software provided by Perkin Elmer. Two distinct temperatures were automatically defined in the thermotropic profiles: the temperature of the onset (T_{on}) and the temperature at the endothermic peak (T_m). To define the range of the phase transition or lateral phase separation (T_f–T_{on}), a third temperature corresponding to the completion of the phase transition (T_f) was determined by extrapolating to the baseline a tangent to the descendent slope of the endothermic peak. These critical transition temperatures were estimated as the mean value of heating scans obtained, at least, from three different samples of the same lipid preparation. To determine the total amount of phospholipid contained in the pans, these were carefully opened at the end of the DSC assay and the lipid was dissolved in chloroform/methanol (3:1) and dried with N_2 flow. Phospholipid content was determined by measuring the inorganic phosphate [23] released after hydrolysis of dried phospholipids, at 180 °C, in 70% $HClO_4$ [24]. The calorimetric enthalpy changes (ΔH) of the thermotropic events, expressed in kcal/mol, were normalized to the exact phospholipid content in each pan.

2.5. SAXS and WAXS

SAXS and WAXS experiments were performed at the beamline A2 of Doris III at HASYLAB (DESY, Hamburg, Germany) with a monochromatic radiation of wavelength 0.15 nm. The SAXS detector was calibrated with rat-tail tendon and the WAXS detector by polyethyleneterephthalat (PET). Heating and cooling scans were performed at a rate of 1 K min^{-1} in the range of 10 °C to 70 °C. Data was recorded for 10 s every min. Static exposures were also taken below and above the main transition temperature of the lipids DPPC and DPPG and only above the main transition temperature of DOPE or the lipid mixture DOPG:DOPE (3:7), and compared at the same temperatures in heating/cooling cycles to check for possible radiation damage. In order to minimize sample exposure to X-ray, a shutter mounted before the sample was kept closed when no data were acquired.

Lamellar lattice distances, d, were calculated from the small angle Bragg reflections using $s = n/d$, where s is the lamellar spacing and n the order of the reflection ($n = 1, 2\ldots$). To obtain a more precise position for s, the diffraction peaks were fitted with Lorentzians and the positions of maximal intensities and peak half-widths at one half of the maximal intensity were determined.

2.6. Fluorescence polarization measurements

The fluorescence polarization measurements of MLV suspensions were performed with a Perkin Elmer LS 55B fluorescence spectrophotometer (Perkin Elmer, U.S.A), equipped with polarization filters and a thermostated cell holder. The excitation wavelength was set at 336 nm and the emission wavelength at 450 nm (5 nm excitation and 6 nm emission band pass) for DPH-PA and at 365 nm and 450 nm for the 2-AS, 6-AS, 12-AS and 16-AP. The fluorescence polarization (P) was calculated according to Shinitzky and Barenholz [25], from the equation

$$P = \frac{I_{II} - GI_{\perp}}{I_{II} + GI_{\perp}},$$

where I_{II} and $I_{\perp}$ are the intensities of the emitted light when the polarizer and analyzer are in the vertical position (I_{II}) or the polarizer is in the vertical and the analyzer in the horizontal position ($I_{\perp}$). The instrumental grating correction factor for the optical system (G) is given by the ratio of the vertically to the horizontally polarized emission components when the excitation light is polarized in the horizontal plane. All fluorescence measurements were corrected for the contribution of light scattering by using appropriate blanks without added fluorescent probes.

The degree of fluorescence polarization reflects probe rotational diffusion and, therefore, reports the structural order or membrane fluidity in the bilayer lipid environments where the probes are embedded. Thus, the term fluidity is operationally used in this work as being inversely proportional to the polarization parameter, and it essentially reflects the rate and the range of motion of phospholipid acyl chains [26].

2.7. Labeling of peptides with nanogold cluster and treatment of cells with peptides

Peptides were tagged with nanogold (Monomaleimido Nanogold, Nanoprobes, NY, d 1.4 nm) as described earlier [27]. A covalent bond was formed between the thiol group of peptide and the maleimide group of label by incubation at a molar ratio 2.5:1 in 50% methanol at 30 °C for 90 min. Methanol was removed and the conjugate concentrated by speed-vac to reach 50–100 μM concentration of labeled peptide. The conjugate with 1:1 peptide/nanogold ratio was purified to homogeneity by size-exclusion chromatography and concentrated.

HeLa cells cultured under standard conditions were seeded onto glass coverslips in 24-well plates, grown to 80–90% confluence and incubated with culture medium containing 1 or 3 μM gold-labeled peptides at 37 °C for 1 h or 4 h. After incubation, the cells were washed twice with cell culture medium and processed for electron microscopy as described earlier [28].

2.8. Statistical analysis of data

The results of DSC and fluorescence polarization are presented as mean ± standard deviation of at least three independent experiments. Multiple comparisons are performed using one-way analysis of variance (ANOVA) with Tukey's multiple pairwise comparison. Statistical significance was set at $p < 0.05$. Errors in experimental values of X-ray diffraction in the determination of d and ξ were assessed based on error estimates of the partial molecular volumes of lipids and water.

3. Results

3.1. Peptides S4(13)-PV_{wt} and S4(13)-PV_{scr} differently affect the thermodynamic properties of zwitterionic (DPPC) and anionic (DPPG) lipid systems

In order to evaluate the effect of the peptides S4(13)-PV_{wt} and S4(13)-PV_{scr} on the thermodynamic properties of lipid bilayers, DSC studies were performed using, as a first approach, liposomes prepared from a single synthetic lipid. A zwitterionic (DPPC) and an anionic phospholipid (DPPG) were used for this purpose and several lipid/peptide molar ratios were assayed, as depicted in Figs. 1 and 2.

According to what has been extensively documented in literature [29], aqueous dispersions of DPPC exhibited two endothermic events (Fig. 1): a pre-transition near 36 °C and a more energetic main

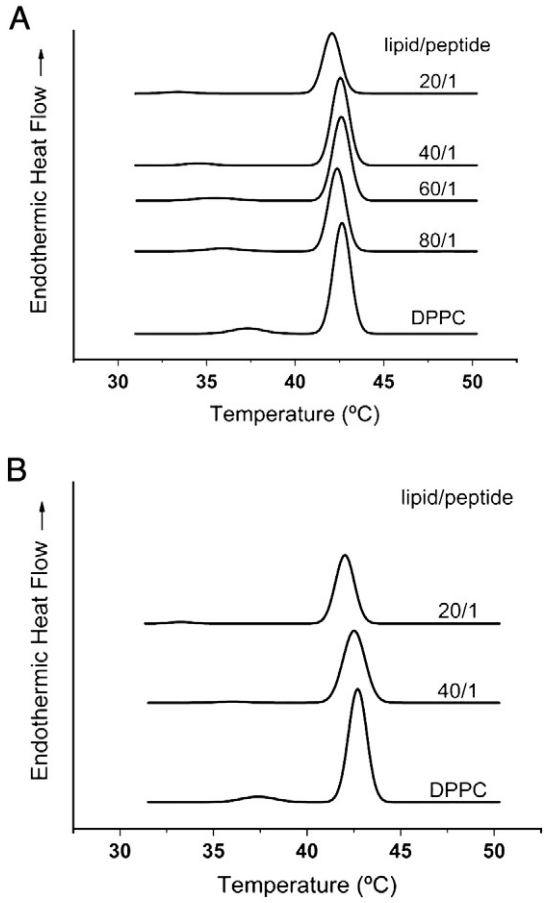

Fig. 1. DSC profiles (heating scans) of DPPC bilayers in the presence of different concentrations of the peptides $S4_{13}$-PV_{wt} (A) and $S4_{13}$-PV_{scr} (B). The lipid/peptide molar ratios are indicated on the scans, which are representative of at least three independent experiments.

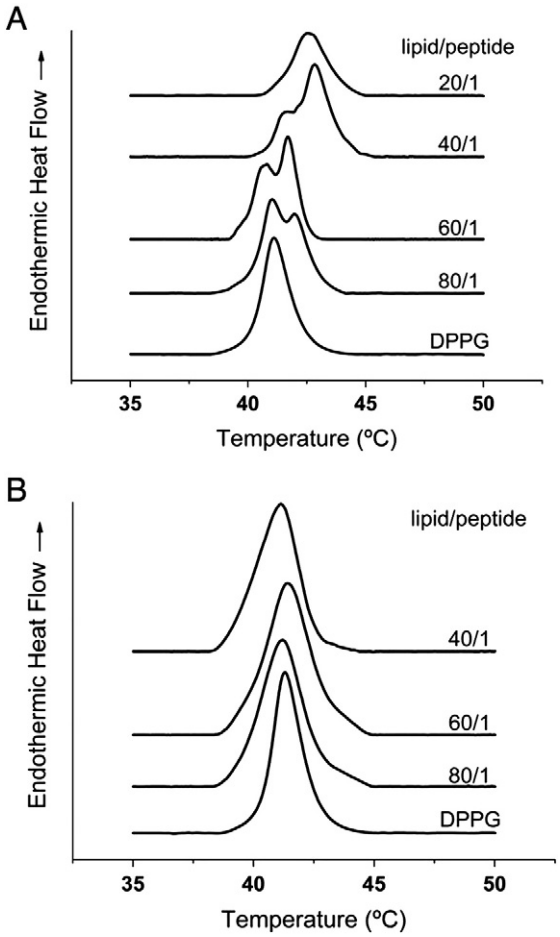

Fig. 2. DSC profiles (heating scans) of DPPG bilayers in the presence of different concentrations of the peptides $S4_{13}$-PV_{wt} (A) and $S4_{13}$-PV_{scr} (B). The lipid/peptide molar ratios are indicated on the scans, which are representative of at least three independent experiments.

transition at around 42 °C. The first endotherm is due to a transition between two gel phases: $L_{\beta'}$, characterized by tightly packed molecules with tilted acyl chains in the *all-trans* conformation and $P_{\beta'}$ phase, where acyl chains are still highly ordered and tilted, but the lipid hydration is enhanced and the bilayer forms periodic membrane ripples [29]. The main transition, whose enthalpy reflects the disruption of van der Waals interactions between the hydrocarbon chains, arises from the conversion of the $P_{\beta'}$ gel phase to a fluid L_{α} phase, where the fatty acid chains are highly disordered due to conformational changes (*trans-gauche* isomerization), the headgroups undergo extensive rotational motion and the whole molecules display lateral diffusion rates of the order of 10^{-8} cm^2 s^{-1}.

In the presence of S4(13)-PV_{wt} or S4(13)-PV_{scr} (Fig. 1 and Table 2), the main phase transition of DPPC liposomes did not show significant alterations. However, the wild-type peptide (Fig. 1A and Table 2) induced a shift of the pre-transition to lower temperatures (from 35.8 °C in the absence of peptide to 33.2 °C at the maximum peptide concentration tested) and a decrease in enthalpy (from 1.14 kcal/mol to 0.24 kcal/mol, in the same conditions). The scrambled peptide (Fig. 1B and Table 2), at a peptide/lipid molar ratio of 1/40, also promoted an enthalpy decrease of the pre-transition of DPPC membranes (to 0.23 Kcal/mol). Since the enthalpy of the main transition was not significantly altered (Table 2), these findings suggest that both peptides did not deeply penetrate the hydrophobic core of DPPC bilayers. However, some interactions might be established between the cationic peptides and the negatively charged phosphate groups of the phospholipids, stabilizing, in the case of the S4(13)-PV_{wt}, the ripple phase, as indicated by the decrease of the pre-transition midpoint.

A distinct scenario resulted from peptide interactions with DPPG membranes displaying a net negative charge (Fig. 2). A pre-transition of DPPG vesicles in media with low ionic strength has been referred in the literature [30]. However, this was not observed with the liposome samples we used for DSC assays, most likely because they were prepared in a salt-containing buffer, reducing the repulsive electrostatic interactions between the phosphate groups and then decreasing the area required for the phospholipid headgroups. In fact, the pre-transition has been registered only with lipids featured by a large area requirement for the polar groups [29]. Therefore, a single endothermic event was observed in our assays, corresponding to the main transition centered at around 41 °C, in agreement with what has been reported in the literature [30]. The wild-type peptide induced a split of this endotherm in two components (Fig. 2A, Table 3), suggesting a non-homogeneous distribution of the peptide within the membrane. The lower temperature component, which is preserved in the lipid/peptide range of 80/1 to 40/1, centered at the temperature of the pure lipid transition, is assigned to less disturbed lipid molecules, which remain in peptide-poor regions. In contrast, the higher temperature component is assigned to lipids residing in peptide-rich domains or those being in closer proximity to peptides, undergoing high perturbation. With increasing concentrations of the peptide, the second peak was progressively favored, leading to a situation (with the higher concentration of peptide tested, 20/1) where the splitting was vanished and only one peak was detected at the highest temperature (42 °C), probably due to a homogeneous lipid population, which is under the influence of peptide molecular interactions. Interestingly, the enthalpy of the main

Table 2
Characterization of the phase transitions detected by DSC (temperature of the endothermic peaks, Tp and Tm, and enthalpy change, ΔH) in liposomes of DPPC in the absence and presence of the peptides $S4_{13}$-PV_{wt} or $S4_{13}$-PV_{scr}, at the lipid/peptide molar ratios indicated in the table.

Peptide type	DPPC/peptide molar ratio	Pre-transition		Main transition	
		T_p (°C)[a]	ΔH (kcal/mol)[a]	T_m (°C)[a]	ΔH (kcal/mol)[a]
No peptide		35.76 ± 0.20	2.4 ± 0.50	42.24 ± 0.34	19.37 ± 1.16
$S4_{13}$-PV_{wt}	80/1	35.70 ± 0.14	0.98 ± 0.34	42.22 ± 0.09	12.28 ± 1.35
	60/1	34.93 ± 0.12	0.97 ± 0.68	42.31 ± 0.20	15.54 ± 2.06
	40/1	34.04 ± 0.42***	0.90 ± 0.33*	42.30 ± 0.20	15.48 ± 3.06
	20/1	33.18 ± 0.12***	0.51 ± 0.32*	42.24 ± 0.25	12.97 ± 2.43
$S4_{13}$-PV_{scr}	40/1	36.49 ± 1.40	0.48 ± 0.40	42.55 ± 0.51	12.99 ± 2.25

[a] These values (means ± standard deviation) were obtained from three DSC experiments. Comparisons were performed in the presence *vs* absence of the peptide (*$p<0.01$, ***$p<0.0001$).

transition of DPPG liposomes in the absence of peptide (ΔH = 5.9 Kcal/mol) was approximately equivalent to the sum of the enthalpies of the two endotherms obtained in peptide-containing preparations at peptide/lipid molar ratios from 80/1 to 60/1 (Table 3). At a peptide/lipid molar ratio of 40/1, the enthalpy of the lower temperature endotherm further decreased, but that of the higher temperature endotherm stopped increasing and, at the maximal peptide/lipid ratio tested (20/1), the enthalpy of the single endotherm was much lower (approximately one half) than that observed in the absence of the peptide. This probably indicates that a fraction of DPPG molecules were somehow "sequestered" by tight interaction with the peptide, being inhibited to participate in the bulk phase transition.

Despite having similar physico-chemical properties (length of the primary sequence, charge and amino acid composition), the scrambled peptide differently affected DPPG model membranes, its action being limited to a concentration-dependent decrease in the enthalpy of the main transition (Fig. 2B and Table 3), which reinforces its different ability to interact and disturb the lipid bilayer.

3.2. Peptides S4(13)-PV_{wt} and S4(13)-PV_{scr} induce structural changes in zwitterionic (DPPC) or anionic (DPPG) lipid systems

The degree of peptide-induced perturbation of the different DPPC phases ($L_{\beta'}$, $P_{\beta'}$ and L_α) at a peptide/lipid molar ratio of 1/50 was evaluated by X-ray diffraction patterns at small and wide angles (SAXS and WAXS), which provide information on the long-range bilayer organization and the hydrocarbon chain packing, respectively.

SAXS (data not shown) and WAXS patterns (Fig. 3A) taken at different temperatures in heating scans allowed the determination of the pre-transition ($L_{\beta'} \rightarrow P_{\beta'}$) and the main transition ($P_{\beta'} \rightarrow L_\alpha$) temperatures of DPPC bilayers (≈35 °C and 42 °C, respectively), which are in agreement with the results obtained by DSC and previously published data [31]. Thus, the WAXS patterns of DPPC, showing two WAXS reflection peaks at 28, 32 and 34 °C (Fig. 3A), are typical of a $L_{\beta'}$ phase with orthorhombic hydrocarbon chain packing. At 36 °C, a broad single Bragg peak was observed, indicating a transition to the $P_{\beta'}$ phase, and the main phase transition occurred at 42 °C, where a defined WAXS peak is no longer visible.

As shown in Fig. 3B and C, the peptides did not alter the main phase transition temperature of DPPC, but promoted some perturbation of the chain packing regarding the $L_{\beta'}$ phase, shifting DPPC pre-transition to lower temperatures (34 °C). This effect, which is particularly evident for the S4(13)-PV_{wt} peptide, corroborates DSC data.

Deconvolution of the WAXS patterns in the $L_{\beta'}$ phase (20 °C) gives the lattice distances of the orthorhombic lattice of the DPPC chain packing, i.e., 4.12 ± 0.05 Å and 4.04 ± 0.05 Å (data not shown), which are also in good agreement with the literature [31]. Neither this chain packing nor the correlation length (ξ) between the bilayers (data not shown) was affected by the presence of the peptides.

A very different scenario was provided by SAXS and WAXS studies with DPPG membranes. It should be emphasized that in these lipid preparations (much more concentrated than those used in DSC assays), it was possible to detect the pre-transition by SAXS and WAXS. The SAXS patterns of DPPG exhibited very diffuse scattering especially at higher temperatures, which results in broad Bragg peaks with low correlation length between the bilayers (ξ). This has been previously observed [32–34] and explained because of the electrostatic repulsion, which leads to the formation of uncorrelated bilayers. DPPG lamellar distances (*d*) determined in each lipid phase are displayed in Table 4. In the $L_{\beta'}$ gel phase, the DPPG bilayer including the water layer showed to be 5.02 ± 0.07 nm thick. Along a heating scan, the spacing increased to 5.76 ± 0.07 nm in the ripple gel phase $P_{\beta'}$, and decreased again to 5.40 ± 0.07 nm in the L_α phase, in a similar fashion to what has been described in the literature [33].

In the presence of S4(13)-PV peptides, no significant effects were denoted in the L_α and $P_{\beta'}$ phases of DPPG bilayers (Table 4). Thus, the position of the Bragg peaks was not altered and *d* values show only a very small increase as compared with pure DPPG bilayers.

However, the addition of peptides led to a lipid phase separation in the $L_{\beta'}$ phase. Hence, the coexistence of a non-affected DPPG gel phase, showing *d* values (≈5.0 nm) not significantly different from those of pure DPPG bilayers, and a phase with much smaller *d* values

Table 3
Characterization of the phase transitions detected by DSC (temperature of the endothermic peak, T_m and enthalpy change, ΔH) in liposomes of DPPG in the absence and presence of the peptides $S4_{13}$-PV_{wt} or $S4_{13}$-PV_{scr}, at the lipid/peptide molar ratios indicated in the table.

Peptide type	DPPG/peptide molar ratio	Main transition			
		T_m (°C)[a]		ΔH (kcal/mol)[a]	
No peptide	–	41.28 ± 0.56	–	5.92 ± 0.17	–
$S4_{13}$-PV_{wt}	80/1	41.22 ± 0.20	42.07 ± 0.13	2.35 ± 3.7	3.03 ± 0.33
	60/1	41.05 ± 0.40	41.82 ± 0.15	2.15 ± 1.70	3.65 ± 1.73
	40/1	41.54 ± 0.30	42.45 ± 0.36	1.65 ± 1.91	3.05 ± 0.74
	20/1	–	42.24 ± 0.32**	–	3.11 ± 1.26
$S4_{13}$-PV_{scr}	80/1	41.48 ± 0.36		4.14 ± 1.20	
	60/1	40.36 ± 1.43		2.68 ± 0.10*	
	40/1	41.38 ± 0.32		2.35 ± 0.17*	

[a] These values (means ± standard deviation) were obtained from three DSC experiments. Comparisons were performed in the presence *vs* absence of the peptide (*$p<0.05$, **$p<0.01$).

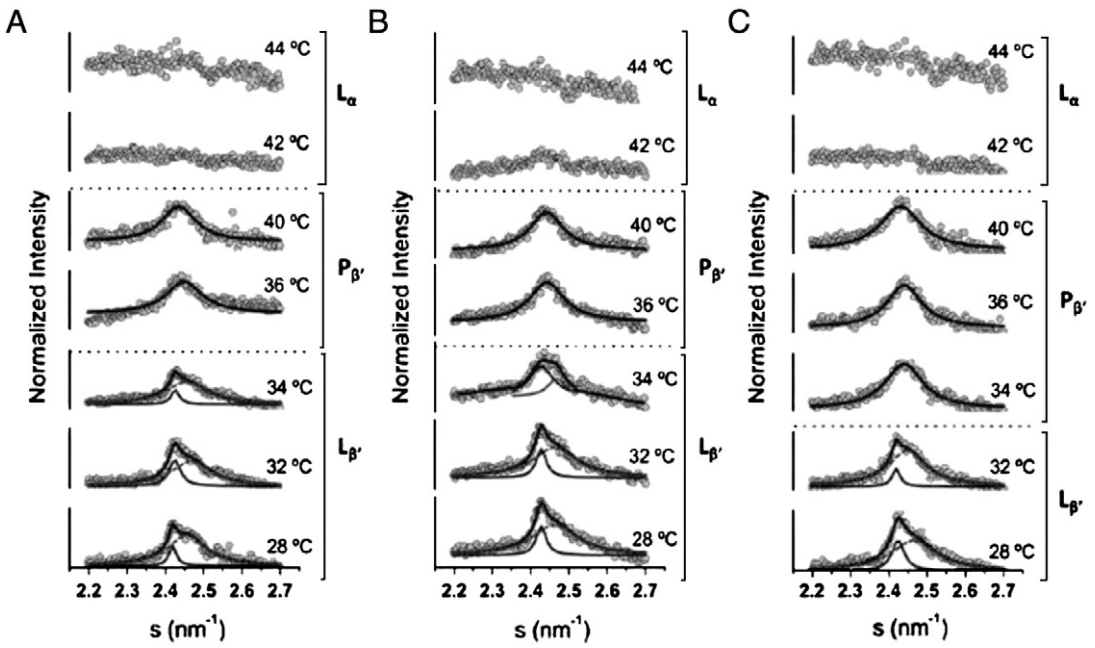

Fig. 3. WAXS patterns of (A) DPPG/$S4_{13}$-PV_{scr} (50/1 molar ratio) and (B) DPPG/$S4_{13}$-PV_{wt} (50/1 molar ratio) at different temperatures. Solid lines give the best fit of the Lorentzian's analysis model to the scattered intensities. Dotted lines represent the transition points observed between $L_{\beta'}$ and $P_{\beta'}$ phases (pre-transition) and between $P_{\beta'}$ and L_α phases (main transition).

(≈3.0 nm), characteristic of a $L_{\beta I}$ interdigitated phase (Table 4), indicates a non-homogeneous distribution of peptides in the most ordered phase ($L_{\beta'}$) of DPPG membranes.

The interdigitated phase visible in the SAXS regime was confirmed in the corresponding WAXS patterns (Fig. 4), which exhibit sharp peaks (gray lines at 10 and 20 °C) in addition to the β′ pattern assigned to an orthorhombic packing of hydrocarbon chains (dashed black lines at 10 and 20 °C). At 38 °C, a single phase was observed again, which is assigned to a ripple phase as indicated by the broad peak, similarly to what was observed in pure DPPG bilayers.

Besides studying the influence of the peptides on each lipid phase, WAXS heating scans were taken at different temperatures to determine the effect of the peptides on the main phase transition temperature ($P_{\beta'} \rightarrow L_\alpha$). Both peptides shifted DPPG main transition to higher temperatures (data not shown), from an ordered to a disordered phase where a defined WAXS peak is no longer visible. Probably peptide-induced broadening of this transition impeded the detection of the temperature upshift in DSC scans in the case of the scrambled peptide (Fig. 2B and Table 3).

Table 4
Long-range distances (d) and correlation length (ξ) determined from SAXS patterns in DPPG bilayers in the absence and in the presence of the peptides $S4_{13}$-PV_{wt} or $S4_{13}$-PV_{scr} (100/1 or 50/1 lipid/peptide molar ratio), at 20, 38 and 50 °C and physiological pH.

Sample	T (°C)/expected lipid phase	d_{SAXS} (Å)		ξ (Å)	
DPPG	20 ($L_{\beta'}$)	50.2 ± 0.7		187 ± 10	
	38 ($P_{\beta'}$)	57.6 ± 0.7		32 ± 15	
	50 (L_α)	54.1 ± 0.7		33 ± 15	
DPPG:$S4_{13}$-PV_{scr} (100/1)	20 ($L_{\beta'}$)	50.4 ± 0.7	36.8 ± 0.7	180 ± 10	140 ± 10
	38 ($P_{\beta'}$)	57.9 ± 0.7		34 ± 15	
	50 (L_α)	54.2 ± 0.7		23 ± 15	
DPPG:$S4_{13}$-PV_{scr} (50/1)	20 ($L_{\beta'}$)	50.4 ± 0.7	36.5 ± 0.7	5 ± 3	18 ± 15
	38 ($P_{\beta'}$)	57.6 ± 0.7		32 ± 15	
	50 (L_α)	54.7 ± 0.7		22 ± 10	
DPPG:$S4_{13}$-PV_{wt} (100/1)	20 ($L_{\beta'}$)	50.7 ± 0.7	37.5 ± 0.7	22 ± 15	105 ± 15
	38 ($P_{\beta'}$)	59.0 ± 0.7		34 ± 15	
	50 (L_α)	54.8 ± 0.7		23 ± 15	
DPPG:$S4_{13}$-PV_{wt} (50/1)	20 ($L_{\beta'}$)	51.7 ± 0.7	37.2 ± 0.7	38 ± 15	114 ± 15
	38 ($P_{\beta'}$)	58.9 ± 0.7		30 ± 15	
	50 (L_α)	54.9 ± 0.7		32 ± 15	

3.3. Peptides S4(13)-PV_{wt} and S4(13)-PV_{scr} alter membrane order parameters monitored at different depths of an anionic lipid (DPPG) system

Fluorescence polarization measurements using fluorescent probes that intercalate at different depths of the lipid bilayer were performed in order to uncover how the S4(13)-PV peptides affect the lateral pressure profile across the thickness of a DPPG membrane. As a first approach, a fluorescence polarization thermogram in DPPG liposomes was obtained with the probe DPH-PA, which monitors the hydrophobic region of the bilayer closer to the surface, at which this molecule is anchored by its negatively charged group [35]. The fluidity-related spectroscopic parameter (P) in DPPG bilayers undergoes, as expected, an abrupt decrease within a relatively narrow temperature range (Fig. 5A), reflecting a sharp phase transition with a temperature midpoint (T_m) at 42 °C, as indicated by the peak of the fluorescence polarization derivative curve (inset in Fig. 5A), in accordance with the above results obtained by DSC and X-ray diffraction. Also consistent with DSC data, both peptides, at a 40/1 lipid/peptide molar ratio, broaden DPPG transition profile, affecting its cooperativity. Additionally, an increase of the order parameter over all the transition temperature range and in the fluid phase was observed (Fig. 5A), this effect being more pronounced for the scrambled peptide. The peptide-induced increase of lipid order may result from the electrostatic interaction between the peptides and the lipid membranes, with a consequent shielding of the surface net charge that might decrease the repulsive forces between the lipid headgroups.

In order to further characterize peptide-induced perturbation across the bilayer thickness, fluorescence polarization studies were performed with n-(9-anthroyloxy) stearic acid (n = 2, 6 and 12) and 16-(9-anthroyloxy) palmitic acid, at lipid/peptide molar ratios of 80/1 and 40/1 and at two different temperatures, one below (12 °C) and other above (60 °C) the DPPG main phase transition (Fig. 5B). For both temperatures, peptide-induced ordering effect was more pronounced in the extremes of the hydrocarbon chains (at the level of carbons 2 and 16 of the stearoyl and palmitoyl chains,

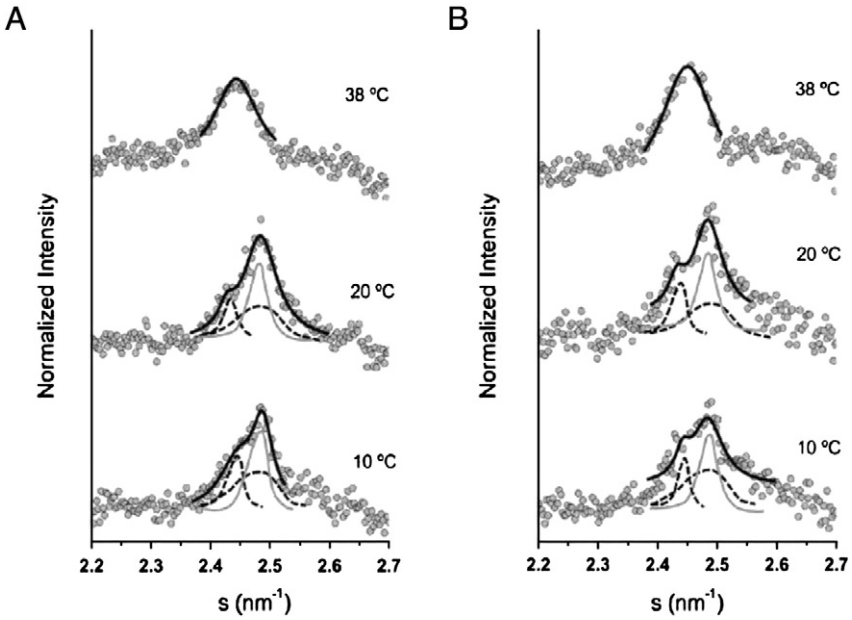

Fig. 4. WAXS patterns of (A) DPPG/$S4_{13}$-PV_{scr} (50/1 molar ratio) and (B) DPPG/$S4_{13}$-PV_{wt} (50/1 molar ratio) at different temperatures. Solid lines give the best fit of the Lorentzian's analysis model to the scattered intensities. At temperatures of 10 and 20 °C the fitting can be described as the superimposition of three peaks corresponding to the orthorhombically packed acyl chains (dashed black lines) and interdigitated acyl chains (gray line).

respectively). This effect was shown to be dependent on peptide concentration and more evident at 12 °C, temperature at which the coexistence of a $L_{\beta'}$ phase and a $L_{\beta I}$ interdigitated phase was demonstrated by the SAXS and WAXS patterns. Peptide-induced broadening of phase transition, as detected by DPH-PA, is also indicative of lateral phase separation.

It should be noted that the interpretation of fluorescence polarization data in these conditions is complicated by the uncertainty of the localization of the fluorescent probes in the plane of the membrane and their preferential distribution between the different coexisting domains. Taking into account these limitations, the increase of fluorescence polarization of 2-AS at temperatures below and above the main phase transition may be a consequence of the interaction of the cationic peptide with the overall negative charges of DPPG headgroups, thus reducing electrostatic repulsion. A tighter packing of lipid molecules would be hence favored in the segment of the hydrocarbon chains closer to the phospholipid polar groups. This effect was not however detected by DPH-PA at 12 °C, probably because this probe monitors the lipid order in a deeper region of the lipid bilayer. On the other hand, the ordering effect induced by the peptide in the hydrophobic core of the bilayer, as monitored by 16-AP, might result from the interdigitation of phospholipid hydrocarbon chains, thus increasing van der Waals interactions.

3.4. The S4(13)-PV_{wt} peptide promotes lipid domain segregation in a POPG/DPPE lipid system

To further characterize peptide–membrane interactions, a binary lipid system containing a partially unsaturated anionic lipid (POPG) and a saturated zwitterionic lipid (DPPE) was used to mimic a physiologically more relevant membrane. The mixture of POPG/DPPE at a molar ratio of 3/7 constitutes a useful model system for DSC studies, since, in spite of the different transition temperatures of its lipid components (−2 °C for POPG and 63 °C for DPPE), it gives rise to a single, yet broad and assymetric peak, which reflects a certain lateral phase separation.

The incorporation of the S4(13)-PV_{wt} peptide into this membrane system produced significant changes in the thermotropic behavior of the lipid mixture (Fig. 6). Relatively low peptide concentrations (lipid/peptide molar ratio of 80/1) promoted an alteration of the DSC profile, giving rise to a shoulder and a peak, which can be assigned to different lipid domains. The peptide apparently induced a displacement of the minor lipid (POPG) to segregated domains, corresponding to the lower melting temperature component (shoulder in the DSC profile). As a consequence, DPPE-enriched domains then exhibit a more cooperative transition, at higher temperatures (the peak in the DSC scan). The lower temperature component seems to shift to higher temperatures as the peptide concentration increased, from 80/1 to 40/1 lipid/peptide molar ratio, suggesting a peptide-induced increase of lipid order. At the highest peptide concentration assayed (20/1), the endotherm became more symmetric, although still comprising two distinct components. Thus, the deconvolution of this peak reflects an effective lateral phase separation between a higher temperature component, assigned to the DPPE-enriched and peptide-poor domains, and a low temperature component, representing the more disordered domains of the anionic lipid POPG to which the peptide preferentially interacts.

3.5. Peptides S4(13)-PV_{wt} and S4(13)-PV_{scr} affect the phase behavior of a DOPG/DOPE lipid system

To evaluate the effect of the peptides S4(13)-PV_{wt} and S4(13)-PV_{scr} on lipid mesomorphism, a mixture of DOPG and DOPE (3/7 molar ratio) was chosen as a model system, since it undergoes a lamellar-to-inverted hexagonal phase ($L_\alpha \rightarrow H_{II}$) transition at temperatures easily available in laboratory [36]. In this context, the ability of the peptides used in this work to induce non-lamellar phases was studied by evaluating their capacity to lower the temperature at which the above lipid mixture undergoes a transition from the lamellar to a non-lamellar phase. As reported in the literature, the L_α phase of DOPG/DOPE mixture (3/7 molar ratio) is stable up to 50 °C, an isotropic phase (I) having been detected by ^{31}P NMR only at temperatures above 60 °C [34]. SAXS studies at 65 °C showed reflections consistent with the formation of a cubic phase (belonging to the space group *Pn3m*) and a small amount of H_{II} phase [36].

In the present work, SAXS measurements were performed at two different temperatures: 20 and 50 °C, where only lamellar phases (L_α) are expected. At the temperatures tested, several small angle

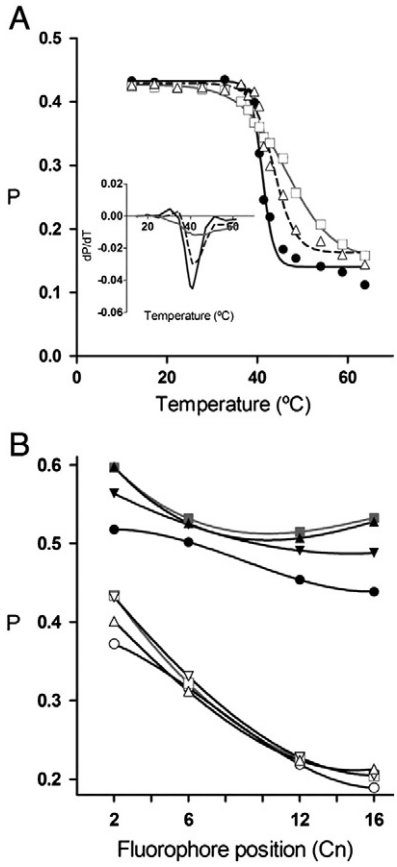

Fig. 5. Fluorescence polarization (P) of DPH-PA (A) or 2-AS, 6-AS, 12-AS and 16-AP (B) in DPPG bilayers in the absence and in the presence of $S4_{13}$-PV_{wt} or $S4_{13}$-PV_{scr}. In A, thermograms were obtained in the absence (●) and in the presence of $S4_{13}$-PV_{wt} (△) or $S4_{13}$-PV_{scr} (□), at a lipid/peptide molar ratio of 40/1. The inset shows the first derivative of the polarization curves. In B, the fluorescence polarization of 2-AS, 6-AS, 12-AS and 16-AP (the carbon number of the stearic or palmitic chain where the 9-anthroyloxy group is attached being represented in the x axis) was measured at 12 °C (filled symbols) and 60 °C (open symbols), in the absence (●, ○) or the presence of $S4_{13}$-PV_{wt} at a lipid/peptide molar ratio of 40/1 (▲, △) and 80/1 (▼, ▽) or $S4_{13}$-PV_{scr} at a lipid/peptide molar ratio of 40/1 (■, □). The results shown are representative of at least three independent experiments.

diffraction peaks were detected in the DOPG/DOPE mixture. The observed reflections in the absence of the peptides are consistent with the coexistence of two lamellar phases: a remaining $L_{\beta'}$ corresponding to the peaks positioned at lower lattice spacings (higher lattice distances in Table 5) and a L_{α} phase corresponding to the peaks positioned at higher lattice spacings (lower lattice distances in Table 5). The first and second order Bragg peaks of each of these lipid phases presented an indexed ratio of 1:2, which indicates the lamellar nature of these phases.

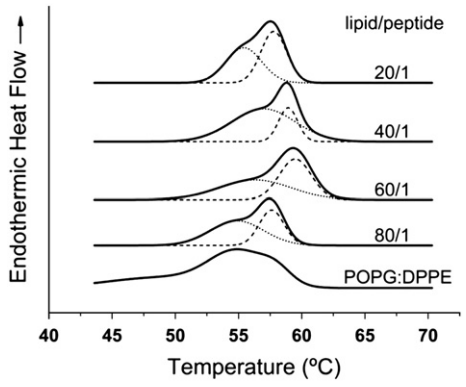

Fig. 6. DSC profiles (heating scans) of POPG/DPPE (3/7 molar ratio) bilayers in the presence of different concentrations of the peptide $S4_{13}$-PV_{wt}. The lipid/peptide molar ratios are indicated on the scans, which are representative of at least three independent experiments.

Concentration-dependent effects were detected upon interaction of either of the two peptides with the lipid mixture. For sake of clarity, only the results obtained with the highest peptide/lipid molar ratio (1/50) are shown. Both peptides showed a significant effect on the lipid mixture phase behavior at this concentration, promoting the formation of more defined Bragg peaks (data not shown) and rising the correlation length (ξ) between the bilayers (Table 5), thus indicating an increase of the lipid order. Moreover, both peptides promoted the formation of non-lamellar phases at lower temperatures (50 °C) than those at which these phases have been reported in this lipid mixture (about 65 °C [36]). In the presence of S4(13)-PV_{scr}, several small angle reflections were observed at 50 °C (Table 5). The first order reflection at 5.06 ± 0.05 nm and the second order reflection at 2.63 ± 0.05 nm were assigned to the lamellar phase (indexed ratio of 1:2), whereas the first order reflections at 4.65 ± 0.05 nm and 5.98 ± 0.05 nm and the second order reflections at 2.63 ± 0.05 nm and 2.97 ± 0.05 nm were assigned to an inverted hexagonal (H_{II}) phase (indexed ratio of 1:√3:2). S4(13)-PV_{wt} peptide also proved to be able to promote the formation of non-lamellar phases, identified in this case as a cubic phase and a small amount of H_{II} phase. Thus, the first order reflections at 4.65 ± 0.05 nm, 5.42 ± 0.05 nm and 6.55 ± 0.05 nm, and the second order reflections at 2.73 ± 0.05 nm and 2.98 ± 0.05 nm (Table 5) were assigned to the cubic phase (indexed ratio of 1:√3:√4:√5) and a H_{II} phase (indexed ratio of 1:√3:2).

3.6. Peptide S4(13)-PV_{wt} induces formation of quasi-hexagonal domains in membranes of HeLa cells

The observation that S4(13)-PV_{wt} peptide was able to affect the phase behavior in a model lipid system prompted us to analyze the interaction of the peptide with the plasma membrane of cells at the ultrastructural level by using transmission electron microscopy. The peptide was tagged for better visualization with nanogold label as described earlier [28] and the electron microscopy studies were performed at peptide concentrations, which would enable a non-endocytotic uptake to occur [20] and could favor lipid transition from a lamellar to a non-lamellar phase. Incubation of HeLa cells with 3 μM labeled wild-type peptide resulted in formation of peptide-containing particles at/on the cell surface (Fig. 7A, B). Analogous structures were not observed with the scrambled peptide (not shown). A closer inspection revealed that the formed particles were not random aggregates but multi-layered and well-structured (Fig. 7A a′, a″ and B b′) with an average distance between layers of 9.5–10 nm. The nanogold label on S4(13)-PV peptide locates between the layers and is detectable as black dots of a non-uniform size with a diameter in the range of 5–15 nm (Fig. 7A a′, a″ and B b′). These findings suggest that the peptide has induced and stabilized the non-lamellar organization of cellular membranes, which is reminiscent of quasi-hexagonal domains [37,38]. The plasma membrane, which is usually very well distinguishable in its lamellar organization in electron micrographs, becomes undetectable (Fig. 7A). However, in some regions of the plasma membrane the formation of non-lamellar lipid phase did not interfere markedly with its regular organization (Fig. 7B).

The peptide-containing structures that resembled quasi-hexagonal domains were very rarely detected on the cell surface at 1 μM S4(13)-PV concentration in parallel with peptide nanoparticles [28]. Whereas the latter were typical and abundant at 1 μM concentration of S4(13)-PV, the former were very seldom found. In addition, the non-lamellar formations detected at 1 μM concentration were always markedly smaller and less organized than those observed at the high peptide concentration. Furthermore, the appearance of quasi-hexagonal domains was a time-dependent process, since such structures were only

Table 5
Long-range distances (d) and correlation length (ξ) determined from SAXS patterns for DOPE:DOPG (7:3) bilayers in the presence of the peptides $S4_{13}$-PV_{wt} or $S4_{13}$-PV_{scr} (50/1 lipid/peptide molar ratio), at 20 and 50 °C and physiological pH.

Sample	T (°C)/expected lipid phase	d_{SAXS} (Å)					ξ (Å)[b]
		1st order diffraction peak			2nd order diffraction peak		
Lipid mixture DOPE:DOPG (7:3)	20 (L_α)	61.3 ± 0.5	47.5 ± 0.5		29.6 ± 0.5	25.6 ± 0.5	33 ± 10
	50 (L_α)	61.3 ± 0.5	50.2 ± 0.5		29.8 ± 0.5	27.1 ± 0.5	43 ± 10
Lipid mixture: $S4_{13}$-PV_{scr} (50:1)	20 (L_α)	61.3 ± 0.5	51.4 ± 0.5		29.7 ± 0.5	26.6 ± 0.5	99 ± 10
	50 (L_α)	59.8 ± 0.5	50.6 ± 0.5	46.5 ± 0.5	29.7 ± 0.5	26.3 ± 0.5	136 ± 10
Lipid mixture: $S4_{13}$-PV_{wt} (50:1)	20 (L_α)	61.0 ± 0.5	57.1 ± 0.5		29.9 ± 0.5	28.5 ± 0.5	539 ± 10
	50 (L_α)	65.5 ± 0.5	54.2 ± 0.5	46.5 ± 0.5	29.8 ± 0.5	27.3 ± 0.5	522 ± 10

detected upon 1 h or longer incubation at the physiological temperature, suggesting the recruitment of specific lipids or slow separation of particular phases in the plasma membrane.

In addition to their presence at the cell surface, the putative non-lamellar structures were found in the membrane of intracellular vesicles, at 3 μM concentration of S4(13)-PV peptide (Fig. 7A a‴). Such peptide-induced arrangements were somewhat surprisingly also observed after incubation of HeLa cells with 1 μM S4(13)-PV (Fig. 8), although the respective structures were markedly smaller and their organization was not as typical as that seen with the peptide at 3 μM concentration. At the low peptide concentration, quasi-hexagonal domains were detected in intracellular vesicles after 4 h incubation (Fig. 8A), although occasionally such structures could also be observed after 1 h (Fig. 8B). Although the SAXS assay demonstrated the induction of the cubic phase in the membrane-mimicking system by the S4(13)-PV peptide, characteristic structures were not detected by electron microscopy after peptide incubation with HeLa cells.

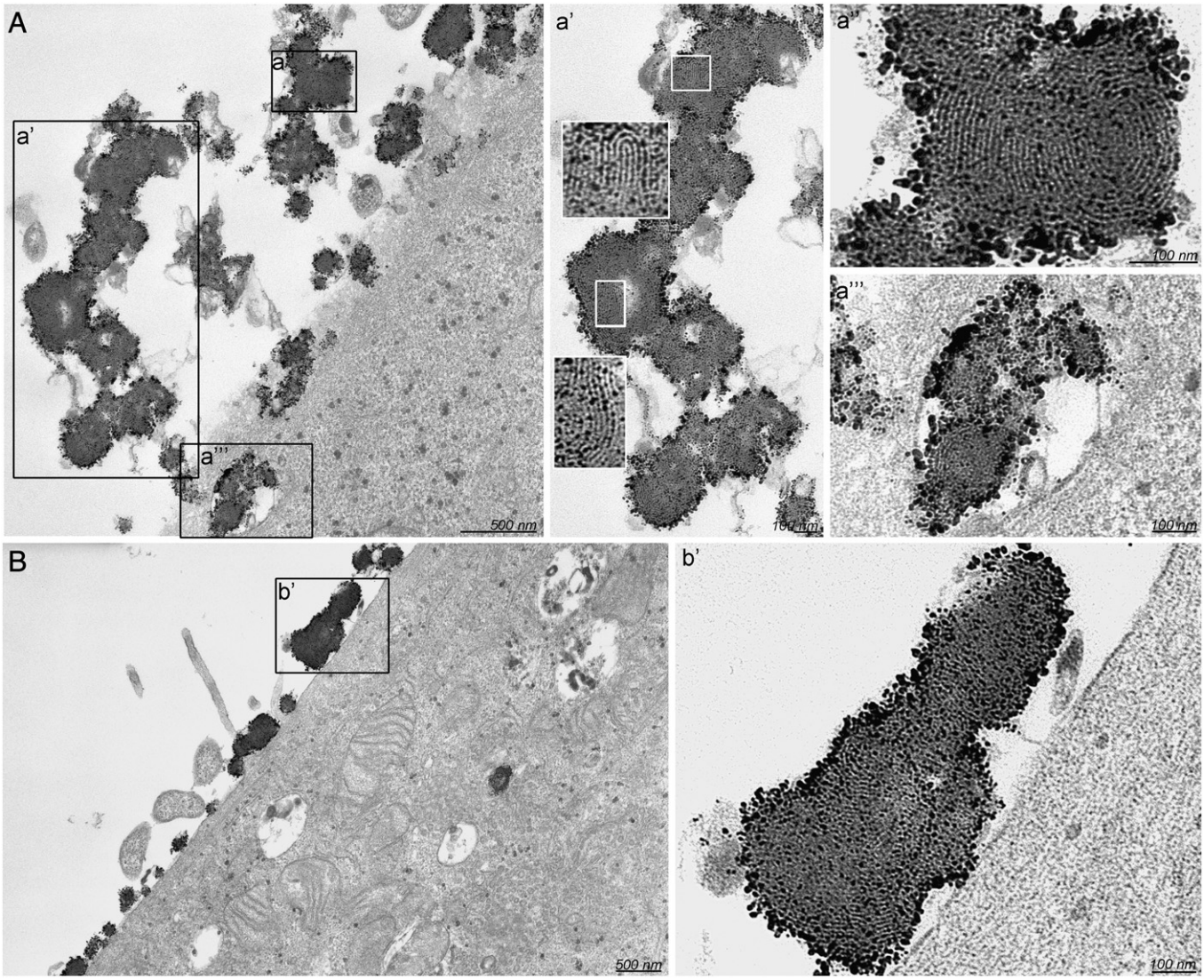

Fig. 7. Transmission electron micrographs showing the interaction of $S4_{13}$-PV_{wt} peptide with plasma membrane of HeLa cells and peptide translocation into the cells. HeLa cells were incubated with 3 μM $S4_{13}$-PV_{wt} during 1 h at 37 °C. Black dots correspond to the nanogold label, visualized by silver enhancement to ~10 nm. $S4_{13}$-PV peptide-containing quasi-hexagonal structures are observed at the surface of HeLa cells (A, B) and their fingerprint pattern is evidenced in enlarged sections (a′, a″, a‴ for image A and b′ for image B).

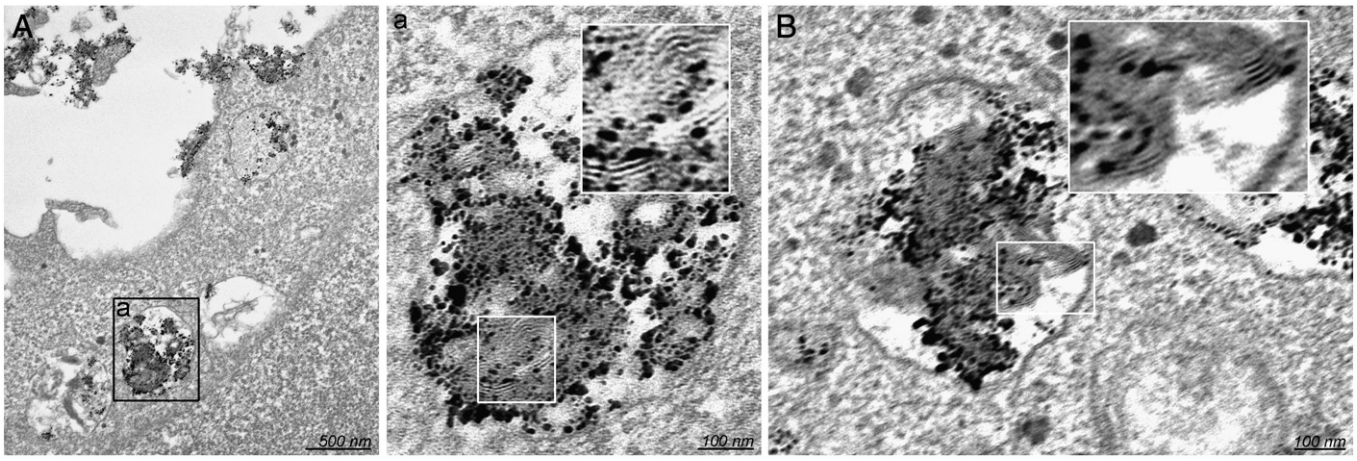

Fig. 8. Transmission electron micrographs showing the interaction of $S4_{13}$-PV_{wt} peptide with the endosomal membrane of HeLa cells. The cells were incubated with 1 μM $S4_{13}$-PV_{wt} for 4 h (A) or 1 h (B), at 37 °C. Black dots correspond to the nanogold label, visualized by silver enhancement to ~10 nm. Quasi-hexagonal domains are detected in intracellular vesicles after 1 h or 4 h incubation and evidenced in enlarged section (a for A image).

4. Discussion

In the field of CPP pharmacological application, the characterization of peptide–membrane interactions has assumed a high relevance to clarify the molecular mechanisms underlying CPP ability to transpose membranes and induce a desirable biological response. In the present work, we focused on the S4(13)-PV peptide and its scrambled analogue, which have been studied in our laboratory showing different capacities to translocate across cell membranes [16] and, accordingly, different competences for nucleic acid delivery [2]. These studies have shown a good correlation between the extent of cellular uptake and the conformational behavior of the peptides upon interaction with negatively charged membrane models [16,19]. In this regard, more efficient internalization of the wild-type peptide has been attributed to its ability to adopt an amphipathic α-helical conformation, whose content increased with the negative charge density of the membrane model. In contrast, the scrambled peptide showed less significant conformational changes, suggesting that the sequence derived from the Dermaseptin S4 peptide [1–13 amino acid residues of the S4(13)-PV_{wt}] is required for the formation of α-helical structures in the presence of negatively charged membranes [19].

Aiming at gaining further insight into the molecular mechanisms responsible for the distinct internalization properties of S4(13)-PV_{wt} and S4(13)-PV_{scr} peptides, we attempted herein to unveil the other side of peptide–membrane interactions, that is, how the physical properties of membrane lipids are affected by each of the peptides.

For reasons of simplicity, we chose as a primary approach membrane models composed of a single synthetic phospholipid, DPPC, because of the relevance of phosphatidylcholine species in eukaryotic plasma membranes, typically found in the outer monolayer of these membranes, or DPPG, which, although rare in mammalian cell membranes, allows to model an anionic membrane mimicking the outer surface of cellular membranes whose negative charges are mainly conferred by gangliosides and proteoglycans.

The minor effects exerted by both peptides on the thermodynamic and structural properties of the neutrally charged DPPC bilayers, in contrast to our observations for the anionic DPPG membranes, as monitored by DSC, fluorescence polarization and X-ray diffraction, evidenced the importance of the electrostatic interactions between the cationic peptide and the lipid headgroups in terms of membrane physical alterations. Therefore, this type of interactions is equally important both from the peptide and the lipid perspective. As mentioned above, the secondary structure of the S4(13)-PV peptide is significantly affected in the presence of vesicles containing negatively charged phospholipids but no conformational changes were observed when neutral membranes are added to the peptide solution in buffer [16]. Moreover, POPC vesicles did not affect the peptide fluorescence emission spectrum, but a blue-shift occurred when the vesicles included increasing amounts of the anionic lipid POPG [19]. Consistently, the intrinsic fluorescence of the S4(13)-PV peptide was efficiently quenched by acrylamide in the presence of neutral lipid vesicles consisting of POPC, in a similar way to that occurring in buffer, but the quenching significantly decreased when increasing amounts of POPG were added to the binary system [16,19]. Overall, these results indicate that electrostatic interactions between the S4(13)-PV peptide and the lipid bilayer are required to trigger a sequence of events: conformational alterations in the peptide followed by its incorporation into the lipid bilayer and, finally, disturbance of membrane physical properties. However, the possibility for perturbations of the membrane structure to occur upon a first contact of the peptide with the membrane surface, due to electrostatic interactions, should not be excluded. In this case, alterations of the lipid environment would be responsible for peptide conformational changes and its insertion into the lipid bilayer. The similar dependence on the presence of negative charges in model membranes observed for the S4(13)-PV_{wt} behavior regarding, on the one hand, its conformational preference and incorporation into the membrane [16,19], and on the other hand, its impact on the physical properties of the bilayer structure, strongly suggests a phenomenological correlation between these two types of events. An identical preference for interacting with anionic versus zwitterionic lipids, affecting the physical properties of the former in a larger extent than the latter, was demonstrated for penetratin [14], an extensively studied CPP, which similarly to the S4(13)-PV_{wt} peptide adopts a helical structure upon interaction with anionic membranes [13]. According to the same authors [14], the electrostatic interaction of the positive charges of penetratin with the anionic lipid headgroups might trigger peptide conformational changes, creating hydrophobic patches in its structure, which prompt the peptide to partially insert into the lipid bilayer.

From the analysis of the differential effects exerted by the wild-type peptide and its scrambled analogue on membranes containing exclusively an anionic lipid (DPPG) or prepared from a mixture of an anionic (POPG or DOPG) and a zwitterionic (DPPE or DOPE) lipid, new insights are gained to explain the mechanisms of cellular uptake for both peptides.

In the simplest model, we emphasize the capacity of the wild-type peptide, not shared by the scrambled analogue, to promote lateral phase separation. This effect denoted in DSC scans, associated to the appearance of an interdigitated phase ($L_{\beta I}$) coexisting with the gel phase characteristic of DPPG pure systems, as revealed by SAXS and WAXS patterns, reflects the capacity of the S4(13)-PV_{wt} peptide to

induce heterogeneities in the lipid matrix of the membrane. As a consequence, defect lines and discontinuities in the boundary of adjacent lipid domains displaying different physical properties may favor peptide insertion into the bilayer and eventual translocation across the bilayer thickness. In contrast, the scrambled peptide, being less efficient in the creation of heterogeneities in the membrane, may have more limited capacity to be taken up by this process. The preferential peptide insertion into defect regions in the bilayer has been demonstrated by atomic force microscopy with an acylated peptide [39] and a mechanism of peptide membrane translocation involving phospholipid segregation has been proposed for penetratin [40].

Data obtained with the binary lipid systems, besides confirming the capacity of the S4(13)-PV_{wt} peptide to promote lipid domain segregation (Fig. 6) also showed peptide capacity to induce non-lamellar phases (Table 5). The isotropic phase detected in the DOPG/DOPE (7:3) mixture at high temperatures has been reported by other authors [36] as corresponding to a cubic phase belonging to the space group Pn3m, with characteristics (hysteretic phase behavior and optical transparency) pointing to a bicontinuous cubic structure. In fact, mixtures composed of a non-bilayer lipid (DOPE in the present case) and a bilayer stabilizer lipid (DOPG in the considered mixture) commonly form this type of structure. Studies with WALP model peptides [40] showed that the formation of the isotropic phase in this lipid system, which is by itself able to form this kind of structure at adequate temperature and water content, is afforded by very low peptide concentrations if an even slight hydrophobic mismatch occurs. This process to induce the lamellar to non-lamellar transition involving reduction of the bilayer rupture tension [41] might be involved in the case of S4 (13)-PV_{wt} peptide. Although the precise hydrophobic length of this peptide is not known, the detection of a $L_{\beta I}$ interdigitated phase in DPPG bilayers in the presence of high peptide/lipid ratios makes the hypothesis of hydrophobic mismatch a reasonable assumption. In fact, the interdigitated phase is commonly triggered to counteract the void volume created in the hydrophobic core of the bilayer as a consequence of the intercalation of molecules featuring a polar group and a short hydrophobic chain (for instance drugs such as ethanol), which does not extend along the full length of the fatty acid chains of phospholipids [42]. Therefore, the interdigitated phase is a solution in conditions where the acyl chains assume the extended (*all-trans*) conformation. However, at higher temperatures, the free space created in the core of the bilayer may induce a higher disorder in the acyl chains leading to an unbalance in the lateral pressure profile across the membrane thickness prone to the formation of non-lamellar phases.

Taking into account that non-lamellar phases have been extensively reported in the literature as being involved in destabilization of the bilayer, increase of membrane permeability and phenomena of membrane fusion and fission [43], it will be easy to infer the impact of these structures, transiently formed in the membrane and at localized regions of the bilayer, on the entry of the S4(13)-PV peptides into the cell. The formation of a non-lamellar phase in DMPG liposomes and the induction of a negative lipid curvature in different lipid systems were also demonstrated in the presence of penetratin [13,14], supporting a mechanism proposed for its translocation [44] which involves inverted micelles entrapping the peptide, crossing the bilayer thickness and releasing it inside the cell.

The current study revealed that besides inducing a non-lamellar organization of lipids in membrane mimicking systems, the S4(13)-PV peptide can propagate and stabilize analogous lipid arrangements (quasi-hexagonal structures) in membranes of HeLa cells, as detected by transmission electron microscopy. In analogy with membrane-mimetic lipid systems, the quasi-hexagonal structures appeared in cell membranes at high peptide to lipid ratios, although not being the prevalent structure. To the best of our knowledge, the formation of non-lamellar structures in cellular membranes upon cell incubation with cell-penetrating peptides has not been reported yet. The inability of the scrambled analogue to promote such membrane alterations would consistently justify its incompetence for delivery. The distinct behavior between the S4(13)-PV wild-type peptide and its scrambled analogue corroborates previous ultrastructural studies [28] which showed that the S4(13)-PV_{wt} peptide assembled in small nanoparticle-like spherical structures upon interaction with the plasma membrane of HeLa cells, whereas the scrambled analogue gave rise to larger irregular aggregates. Although the formation of nanoparticle-regular structures seemed to firstly involve peptide association with the cell surface anionic glycosaminoglycans (GAG), it was observed that nanoparticles were formed even on the surface of a mutant cell line derived from CHO-K1 (pgs A-745), which lacks the capacity to synthesize proteoglycans, due to a deficiency in xylosyltransferase I, involved in GAG biosynthesis. Consistently, previous studies with this cell line and the corresponding wild type (CHO-K1) using flow cytometry and confocal microscopy [20] showed that the peptide concentration was determinant for the role played by proteoglycans in S4(13)-PV cellular internalization. Thus, while at low peptide concentrations ($\leq$1 μM) the cellular uptake was significantly decreased in cells lacking proteoglycans (pgs A-745), at higher concentrations (2.0 μM) peptide uptake by these cells was not significantly different from that observed in the wild-type cells. In the present work, the mechanisms underlying the successful cell internalization of the S4(13)-PV peptide, as opposed to the scrambled analogue, were investigated in conditions (high peptide concentrations) at which the peptide is taken up by an energy-independent pathway and a GAG-non-requiring process, focusing in particular on the membrane lipid component and peptide effects on its mesomorphic behavior.

Considering the whole set of our results, describing the S4(13)-PV peptide interactions with lipid membranes in terms of the consequences for both the peptide and the lipid component, we propose that electrostatic interactions with negatively charged phospholipid headgroups should trigger two kinds of events: change in peptide conformation, adopting an amphipathic α-helix, and lateral separation of lipid domains with different physical properties, creating conditions for generating non-lamellar lipid phases. Non-bilayer phases could be favored by an eventual mismatch between the hydrophobic lipid matrix and the hydrophobic peptide length.

At the cell surface, the negative charges should be provided by proteoglycans or gangliosides, which with other lipids (saturated phospholipids and cholesterol) form specific domains in the plasma membrane (lipid rafts) of a liquid-ordered phase characterized by a high conformational order but relatively low constraints in molecular lateral diffusion. Lateral phase separation and rearrangement of lipid organization and distribution in the plane of the membrane, as a consequence of peptide–lipid interactions, are also predictable and peptide incorporation through defect zones in the interfacial boundaries of lipid domains will be easily achieved. Subsequent alterations of bilayer thickness, undulations and changes in membrane curvature may also occur and have been proposed to be involved in the translocation of other CPPs [40].

5. Conclusion

In conclusion, data obtained so far with S4(13)-PV peptides provide important details on the mechanism of action of these CPPs and may be useful for other amphipathic peptides. It should be emphasized that insights gained by the use of complementary biophysical techniques and transmission electron microscopy could be helpful for understanding the molecular mechanisms of membrane physical modulation by external agents, and can constitute a successful approach to clarify the specificity of biological responses triggered by apparently similar molecules. In terms of cell-penetrating peptides, it should be stressed that peptide interactions with the phospholipid matrix play a determinant role in the success of their pharmacological application and should be taken into account in the design of novel molecules.

Acknowledgements

This work was supported by the grants PTDC/QUI-BIQ/103001/2008 and PTDC/BIO/65627/2006, funded by the Portuguese Foundation for Science and Technology and COMPETE and FEDER and by grants from the Estonian Science Foundation (ESF 7058) and the Estonian Ministry of Education and Research (0180019s11). A.C. is a recipient of a fellowship from the Portuguese Foundation for Science and Technology (SFRH/BD/63288/2009). A.L was supported by European Social Fund's Doctoral Studies and Internationalisation Program DoRa, and is the recipient of the EMBO short-term fellowship.

References

[1] M.C. Morris, S. Deshayes, F. Heitz, G. Divita, Cell-penetrating peptides: from molecular mechanisms to therapeutics, Biol. Cell 100 (2008) 201–217.
[2] S. Trabulo, A.L. Cardoso, M. Mano, M.C. Pedroso de Lima, Cell-penetrating peptides—mechanisms of cellular uptake and generation of delivery systems, Pharmaceuticals 3 (2010) 961–993.
[3] G. Tunnemann, R.M. Martin, S. Haupt, C. Patsch, F. Edenhofer, M.C. Cardoso, Cargo-dependent mode of uptake and bioavailability of TAT-containing proteins and peptides in living cells, FASEB J. 20 (2006) 1775–1784.
[4] S. Trabulo, S. Resina, S. Simoes, B. Lebleu, M.C. Pedroso de Lima, A non-covalent strategy combining cationic lipids and CPPs to enhance the delivery of splice correcting oligonucleotides, J. Control. Release 145 (2010) 149–158.
[5] L. Crombez, G. Aldrian-Herrada, K. Konate, Q.N. Nguyen, G.K. McMaster, R. Brasseur, F. Heitz, G. Divita, A new potent secondary amphipathic cell-penetrating peptide for siRNA delivery into mammalian cells, Mol. Ther. 17 (2009) 95–103.
[6] S. Trabulo, M. Mano, H. Faneca, A.L. Cardoso, S. Duarte, A. Henriques, A. Paiva, P. Gomes, S. Simoes, M.C. de Lima, S4(13)-PV cell penetrating peptide and cationic liposomes act synergistically to mediate intracellular delivery of plasmid DNA, J. Gene Med. 10 (2008) 1210–1222.
[7] A. Pfeifer, I.M. Verma, Gene therapy: promises and problems, Annu. Rev. Genomics Hum. Genet. 2 (2001) 177–211.
[8] S. Simões, A. Filipe, H. Faneca, M. Mano, N. Penacho, N. Düzgünes, M. Pedroso de Lima, Cationic liposomes for gene delivery, Expert Opin. Drug Deliv. 2 (2005) 237–254.
[9] T. Niidome, L. Huang, Gene therapy progress and prospects: nonviral vectors, Gene Ther. 9 (2002) 1647–1652.
[10] G. Vereb, J. Szollosi, J. Matko, P. Nagy, T. Farkas, L. Vigh, L. Matyus, T.A. Waldmann, S. Damjanovich, Dynamic, yet structured: the cell membrane three decades after the Singer–Nicolson model, Proc. Natl. Acad. Sci. U. S. A. 100 (2003) 8053–8058.
[11] C. Peetla, A. Stine, V. Labhasetwar, Biophysical interactions with model lipid membranes: applications in drug discovery and drug delivery, Mol. Pharm. 6 (2009) 1264–1276.
[12] S.R. Dennison, R.D. Baker, I.D. Nicholl, D.A. Phoenix, Interactions of cell penetrating peptide Tat with model membranes: a biophysical study, Biochem. Biophys. Res. Commun. 363 (2007) 178–182.
[13] I.D. Alves, N. Goasdoue, I. Correia, S. Aubry, C. Galanth, S. Sagan, S. Lavielle, G. Chassaing, Membrane interaction and perturbation mechanisms induced by two cationic cell penetrating peptides with distinct charge distribution, Biochim. Biophys. Acta 1780 (2008) 948–959.
[14] I.D. Alves, I. Correia, C.Y. Jiao, E. Sachon, S. Sagan, S. Lavielle, G. Tollin, G. Chassaing, The interaction of cell-penetrating peptides with lipid model systems and subsequent lipid reorganization: thermodynamic and structural characterization, J. Pept. Sci. 15 (2009) 200–209.
[15] P. Guterstam, F. Madani, H. Hirose, T. Takeuchi, S. Futaki, S. El Andaloussi, A. Graslund, U. Langel, Elucidating cell-penetrating peptide mechanisms of action for membrane interaction, cellular uptake, and translocation utilizing the hydrophobic counter-anion pyrenebutyrate, Biochim. Biophys. Acta 1788 (2009) 2509–2517.
[16] M. Mano, A. Henriques, A. Paiva, M. Prieto, F. Gavilanes, S. Simoes, M.C. Pedroso de Lima, Cellular uptake of S4(13)-PV peptide occurs upon conformational changes induced by peptide–membrane interactions, Biochim. Biophys. Acta 1758 (2006) 336–346.
[17] Z. Arsov, M. Nemec, M. Schara, H. Johansson, U. Langel, M. Zorko, Cholesterol prevents interaction of the cell-penetrating peptide transportan with model lipid membranes, J. Pept. Sci. 14 (2008) 1303–1308.
[18] K.J. Hallock, D.K. Lee, J. Omnaas, H.I. Mosberg, A. Ramamoorthy, Membrane composition determines pardaxin's mechanism of lipid bilayer disruption, Biophys. J. 83 (2002) 1004–1013.
[19] M. Mano, A. Henriques, A. Paiva, M. Prieto, F. Gavilanes, S. Simoes, M.C. de Lima, Interaction of S413-PV cell penetrating peptide with model membranes: relevance to peptide translocation across biological membranes, J. Pept. Sci. 13 (2007) 301–313.
[20] M. Mano, C. Teodosio, A. Paiva, S. Simoes, M.C. Pedroso de Lima, On the mechanisms of the internalization of S4(13)-PV cell-penetrating peptide, Biochem. J. 390 (2005) 603–612.
[21] G.B. Fields, R.L. Noble, Solid phase peptide synthesis utilizing 9-fluorenylmethoxycarbonyl amino acids, Int. J. Pept. Protein Res. 35 (1990) 161–214.
[22] A.S. Jurado, T.J. Pinheiro, V.M. Madeira, Physical studies on membrane lipids of *Bacillus stearothermophilus* temperature and calcium effects, Arch. Biochem. Biophys. 289 (1991) 167–179.
[23] G.R. Bartlett, Phosphorus assay in column chromatography, J. Biol. Chem. 234 (1959) 466–468.
[24] C.J.F. Böttcher, C.M. van Gent, C. Pries, A rapid and sensitive sub-microphosphorus determination, Anal. Chim. Acta 24 (1961) 203–204.
[25] M. Shinitzky, Y. Barenholz, Fluidity parameters of lipid regions determined by fluorescence polarization, Biochim. Biophys. Acta 515 (1978) 367–394.
[26] B.R. Lentz, Membrane fluidity as detected by diphenylhexatriene probes, Chem. Phys. Lipids 50 (1989) 171–190.
[27] C. Palm-Apergi, A. Lorents, K. Padari, M. Pooga, M. Hällbrink, The membrane repair response masks membrane disturbances caused by cell-penetrating peptide uptake, FASEB J. 23 (2009) 214–223.
[28] K. Padari, K. Koppel, A. Lorentz, M. Hallbrink, M. Mano, M.C. Pedroso-Lima, M. Pooga, $S4_{13}$-PV cell-penetrating peptide forms nanoparticle-like structures to gain entry into cells, Bioconjug. Chem. 21 (2010) 774–783.
[29] R.B. Gennis, Biomembranes, Molecular Structure and Function, Springer-Verlag, New York Inc., 1989
[30] D.A. Wilkinson, T.J. McIntosh, A subtransition in a phospholipid with a net charge, dipalmitoylphosphatidylglycerol, Biochemistry 25 (1986) 295–298.
[31] M. Lucio, F. Bringezu, S. Reis, J.L. Lima, G. Brezesinski, Binding of nonsteroidal anti-inflammatory drugs to DPPC: structure and thermodynamic aspects, Langmuir 24 (2008) 4132–4139.
[32] S. Danner, G. Pabst, K. Lohner, A. Hickel, Structure and thermotropic behavior of the *Staphylococcus aureus* lipid lysyl-dipalmitoylphosphatidylglycerol, Biophys. J. 94 (2008) 2150–2159.
[33] G. Pabst, S. Danner, S. Karmakar, G. Deutsch, V.A. Raghunathan, On the propensity of phosphatidylglycerols to form interdigitated phases, Biophys. J. 93 (2007) 513–525.
[34] F. Prossnigg, A. Hickel, G. Pabst, K. Lohner, Packing behaviour of two predominant anionic phospholipids of bacterial cytoplasmic membranes, Biophys. Chem. 150 (2010) 129–135.
[35] P.J. Trotter, J. Storch, 3-[p-(6-phenyl)-1,3,5-hexatrienyl]phenylpropionic acid (PA-DPH): characterization as a fluorescent membrane probe and binding to fatty acid binding proteins, Biochim. Biophys. Acta 982 (1989) 131–139.
[36] S. Morein, I.R. Koeppe, G. Lindblom, B. de Kruijff, J.A. Killian, The effect of peptide/-lipid hydrophobic mismatch on the phase behavior of model membranes mimicking the lipid composition in *Escherichia coli* membranes, Biophys. J. 78 (2000) 2475–2485.
[37] D.P. Siegel, W.J. Green, Y. Talmon, The mechanism of lamellar-to-inverted hexagonal phase transitions: a study using temperature-jump cryo-electron microscopy, Biophys. J. 66 (1994) 402–414.
[38] D.P. Siegel, R.M. Epand, The mechanism of lamellar-to-inverted hexagonal phase transitions in phosphatidylethanolamine: implications for membrane fusion mechanisms, Biophys. J. 73 (1997) 3089–3111.
[39] T.B. Pedersen, T. Kaasgaard, M.O. Jensen, S. Frokjaer, O.G. Mouritsen, K. Jorgensen, Phase behavior and nanoscale structure of phospholipid membranes incorporated with acylated C14-peptides, Biophys. J. 89 (2005) 2494–2503.
[40] A. Lamaziere, O. Maniti, C. Wolf, O. Lambert, G. Chassaing, G. Trugnan, J. Ayala-Sanmartin, Lipid domain separation, bilayer thickening and pearling induced by the cell penetrating peptide penetratin, Biochim. Biophys. Acta 1798 (2010) 2223–2230.
[41] E. Evans, D. Needham, Physical properties of surfactant bilayer membranes: thermal transitions, elasticity, rigidity, cohesion and colloidal interactions, J. Phys. Chem. 91 (1987) 4219–4228.
[42] P. Nambi, E.S. Rowe, T.J. McIntosh, Studies of the ethanol-induced interdigitated gel phase in phosphatidylcholines using the fluorophore 1,6-diphenyl-1,3,5-hexatriene, Biochemistry 27 (1988) 9175–9182.
[43] V. Luzzati, H. Delacroix, A. Gulik, T. Gulik-Krzywicki, P. Mariani, R. Vargas, Cubic phases of lipids, in: R.M. Epand (Ed.), Lipid Polymorphism and Membrane Properties, Current Topics in Membranes, Vol. 40, Academic Press, New York, 1997, pp. 3–24.
[44] D. Derossi, G. Chassaing, A. Prochiantz, Trojan peptides: the penetratin system for intracellular delivery, Trends Cell Biol. 8 (1998) 84–87.